Electronic Supplementary Material (ESI) for Nanoscale.

Supporting Information

# Hybrid plasmonic nanostructures based on controlled integration of $MoS_2$ flakes on metallic nanoholes

*Denis Garoli*, Dario Mosconi, Ermanno Miele, Nicolò Maccaferri, Matteo Ardini, Giorgia Giovannini, Michele Dipalo, Stefano Agnoli and Francesco De Angelis*

D. Garoli, E. Miele, N. Maccaferri, M. Ardini, G. Giovannini, M. Dipalo, F. De Angelis
Istituto Italiano di Tecnologia, via Morego 30, I-16163, Genova, Italy.
E-mail: denis.garoli@iit.it
D. Mosconi, S. Agnoli
Dipartimento di Chimica, Università degli Studi di Padova, Via Marzolo 1, 35131 Padova, Italy.

Keywords: Self-organized formation, $MoS_2$, nanopore, plasmonic nanopore, optical antennae, Raman enhancement.

## 1. Preparation and characterization of $MoS_2$ flakes

### Exfoliation of $MoS_2$

In a glove-box (water < 1 ppm, $O_2$ < 10 ppm), $LiBH_4$ (0.109 g, 5 mmol) and $MoS_2$ (0.320 g, 2 mmol) were grounded in a mortar and subsequently transferred in a Schlenk-tube, which then was brought outside of the glove-box and connected to a Schlenk-line. This mixture was heated in a sand bath at 330°C for 4 days under nitrogen. Afterwards, the Schlenk-tube was brought again inside the dry-box, where it was newly grounded with additional $LiBH_4$ (0.109 g, 5 mmol). The sample was subsequently heated for 3 days at 330°C under nitrogen.

The intercalation product was added in a single shot in 270 ml of degassed water and the resulting suspension was bath-sonicated for 1 h to facilitate the exfoliation.

In order to remove the LiOH produced, the suspension was equally divided into six centrifugation tubes (45 ml/tube) and centrifuged at 10000 rpm (23478*g*) for 20 min for three times, replacing the supernatant with clean solvent.

To select the flake size, the suspension purified by LiOH, was progressively centrifuged at 8000 (15026*g* – 8K fraction), 6000 (8452*g* – 6K), 4000 (3757*g* – 4K), 3000 (2113*g* – 3K), 2000 (939*g* – 2K) and 1000 rpm (235*g* – 1K), by collecting each time the top 2/3 of the supernatant and by replacing it with ultrapure water. (Fig. S2).

### Characterization

Scanning electron microscopy (SEM) measurements were performed using a field emission source equipped with a GEMINI column (Zeiss Supra VP35). The micrographs were obtained using an acceleration voltage of 5 kV using the InLens detector of the instrument. The samples were prepared from suspensions diluted with ethanol and drop-casted on Au-coated Si wafers (Fig. S1).

X-ray Photoemission Spectroscopy (XPS) data were acquired in a custom designed UHV system equipped with an EA 125 Omicron electron analyzer with five channeltrons, working at a base pressure of $10^{-9}$ mbar (Fig. S3). The core level photoemission spectra were taken using Mg anode of a conventional non-monochromatized X-ray source (Kα=1253.6 eV). The electron analyser pass energy was set to 50 eV for the survey wide scans and to 20 eV for the single spectral region (Mo3d and S2p). The measurements were accomplished at r.t. in normal emission. The samples were prepared by drop casting the as-produced suspensions on a copper disk and drying the solvent under vacuum.

The characterization by Raman spectroscopy was performed using ThermoFisher DXR Raman microscope. The spectra were recorded directly on small drops using a laser with an excitation wavelength of 532 nm (8 mW), focused on the sample with a 50× objective (Olympus).

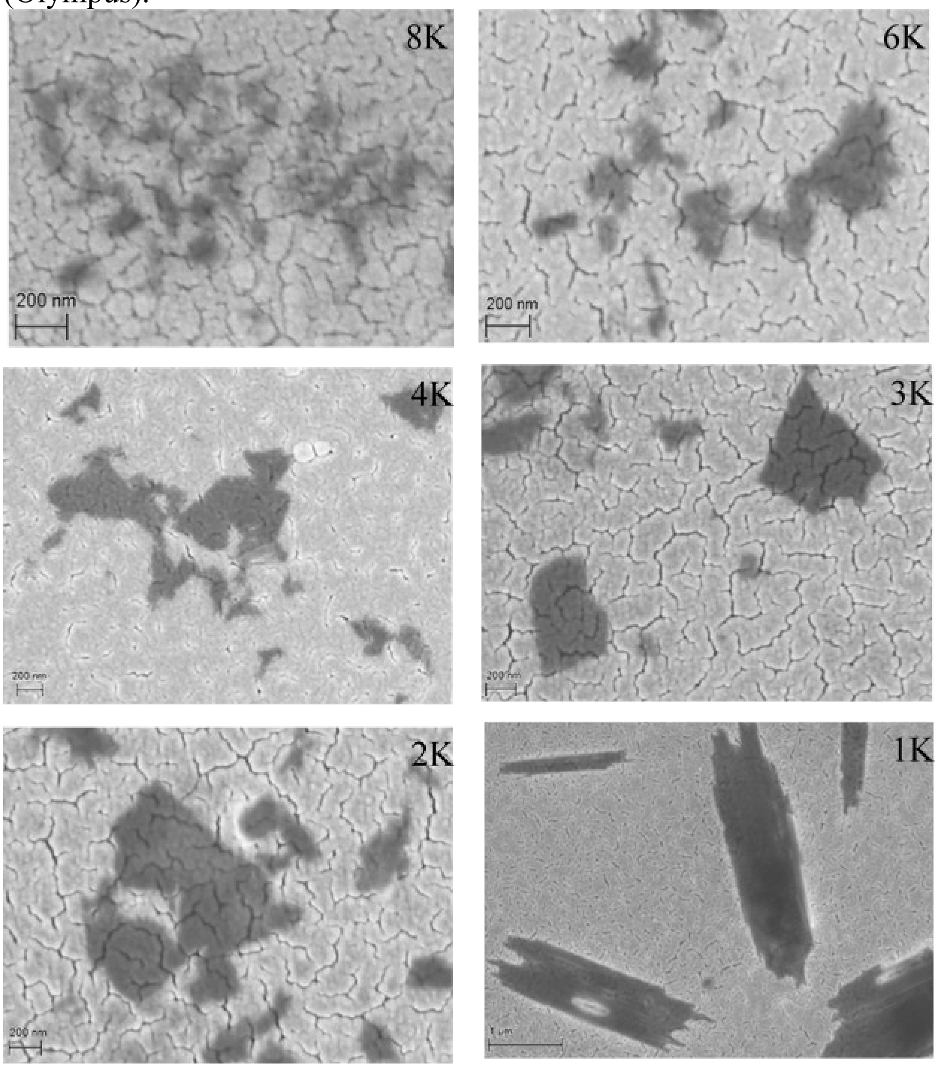

**Figure S1.** *SEM micrographs for chemically exfoliated $MoS_2$ nanoscheets separated at different centrifugations speeds as reported on the top right corner of each panel.*

$MoS_2$ nanosheet size distribution:

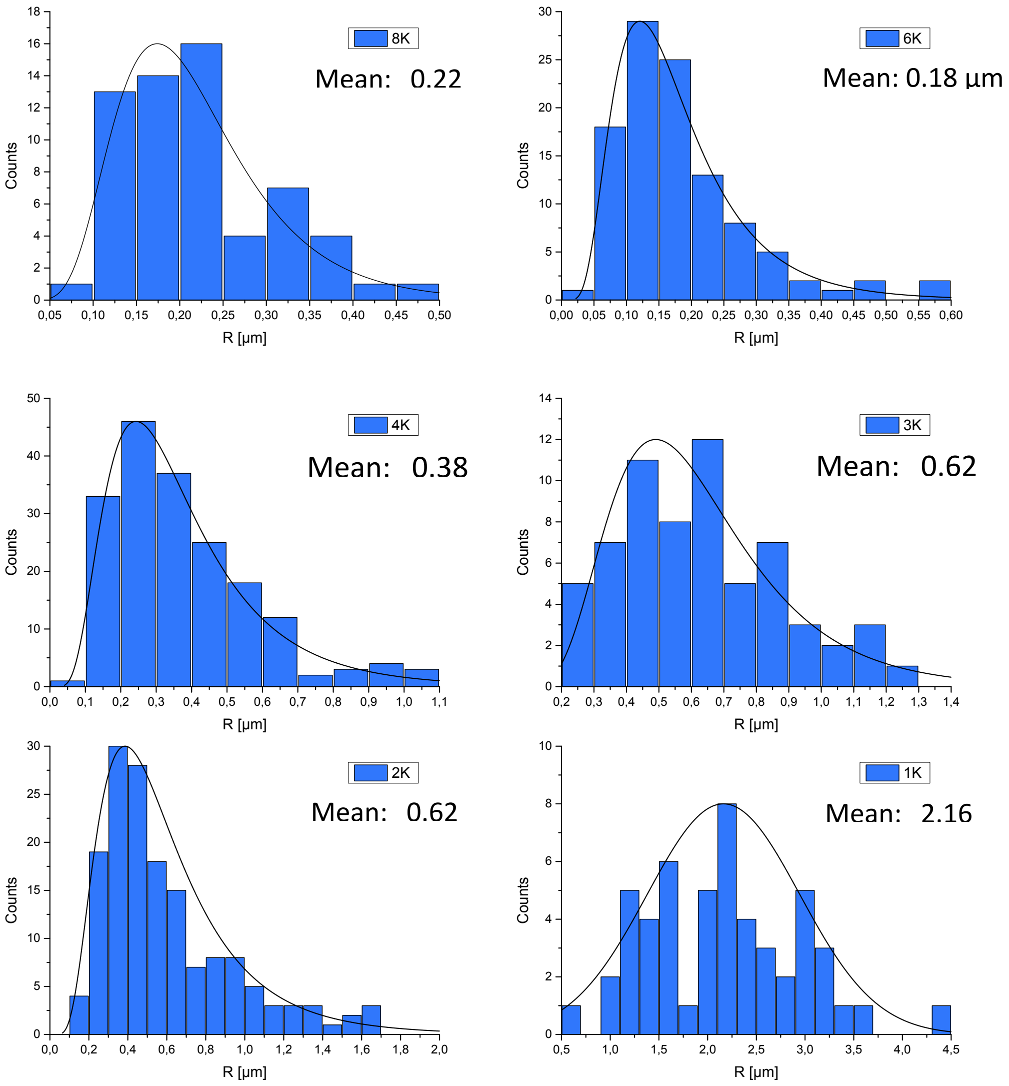

**Figure S2.** *Size distribution calculated from SEM analysis.*

Photoemission spectra of the materials before and after Li intercalation and exfoliation processes were separated into chemically shifted components (Fig. S3). For bulk $MoS_2$, in the Mo 3d photoemission line we recognize the typical features of this material, which are a main doublet at 229.1 eV, assigned to the semiconducting 2H-phase, and a minor one at 232.1 eV due to surface Mo (VI) oxides (3% of total Mo content) (Fig. S3-A). The S 2p present only one component at 161.7 eV, which is ascribed to S2- species (Fig. S3-B). After the exfoliation, the Mo 3d region shows a clear shift due to the phase change from the semiconducting 2H to the metallic 1T phase. In this case, the Mo 3d spectrum was fit with an additional peak at 228.1 eV corresponding to the 1T phase (Fig. S3-C). The final composition was determined to be 77.5% 1T-$MoS_2$, 17.6% 2H-$MoS_2$ and 4.9% $MoO_3$. Also in the S 2p deconvolution, a second component had to be added (160.8 eV) because of the phase change (Fig. S3-D). The theoretical S/Mo stoichiometric ratio is maintained for both materials, with values of 2.0 for bulk material and 2.1 after exfoliation.

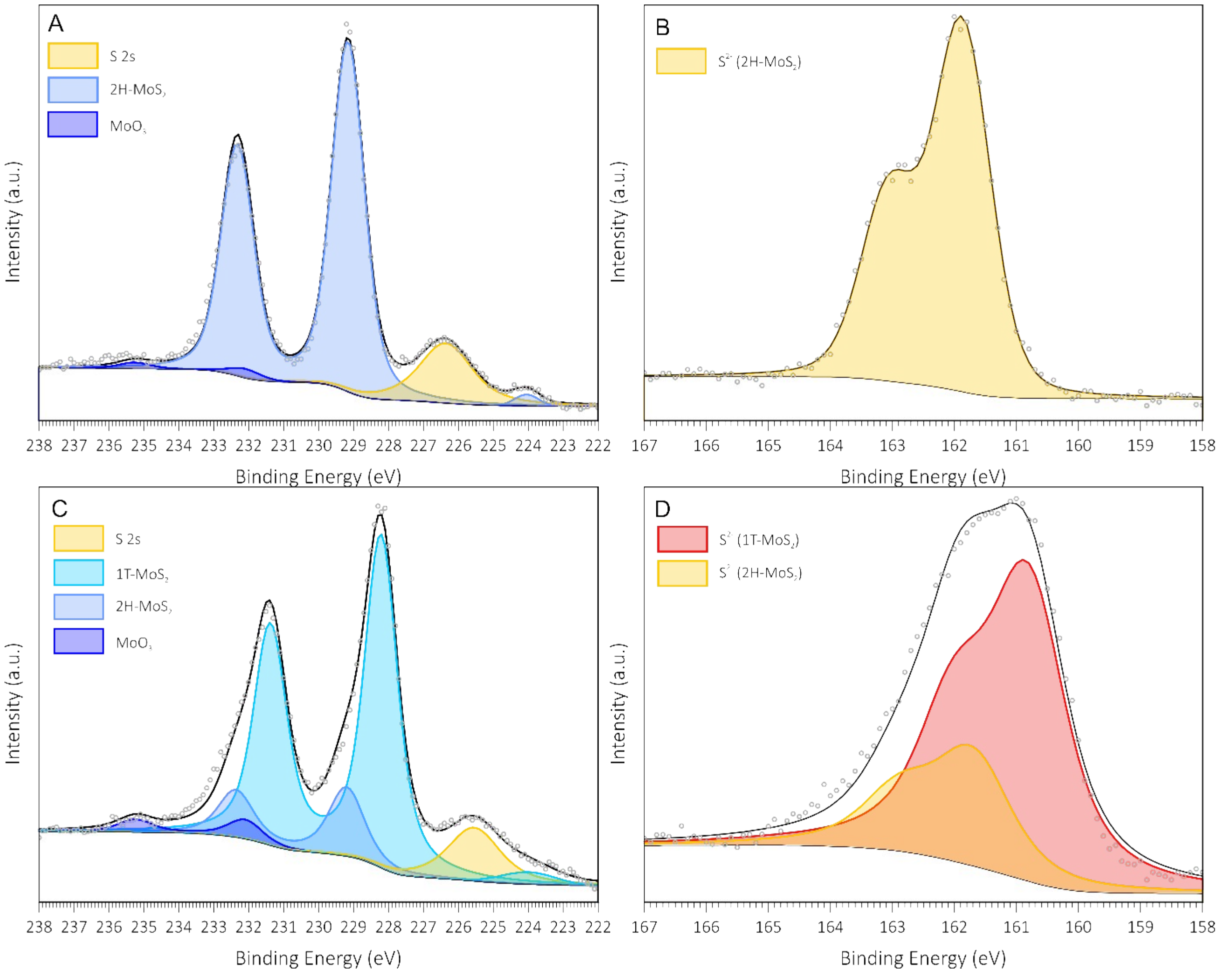

**Figure S3.** *Mo 3d and S 2p photoemission lines for commercial bulk $MoS_2$ powder (A and B) and for exfoliated $MoS_2$ (C and D).*

## 2. FEM Simulation of MoS2 flakes integrated over plasmonic nanohole

The plasmonic effect that can be exploited in the obtained structures has been investigated also on metallic nanoholes integrated with $MoS_2$ flakes. We investigate the plasmonic properties of the structure by means of finite element method (FEM) simulations by using of the RF Module in Comsol Multiphysics taking into account the fabricated geometry. Here we consider a hole of 100 nm diameter into $Si_3N_4$//Au 50//50 nm membrane. It's well known that such a nanohole can confine the electromagnetic field (Fig. S4(a)) and this is also the case when a $MoS_2$ layer is placed on the top (Fig. S4(b)). As can be seen the obtained enhancement is significantly lower respect to the case of 3D antenna also when a nanohole of 5 nm into the $MoS_2$ is considered (Fig. S4(c)).

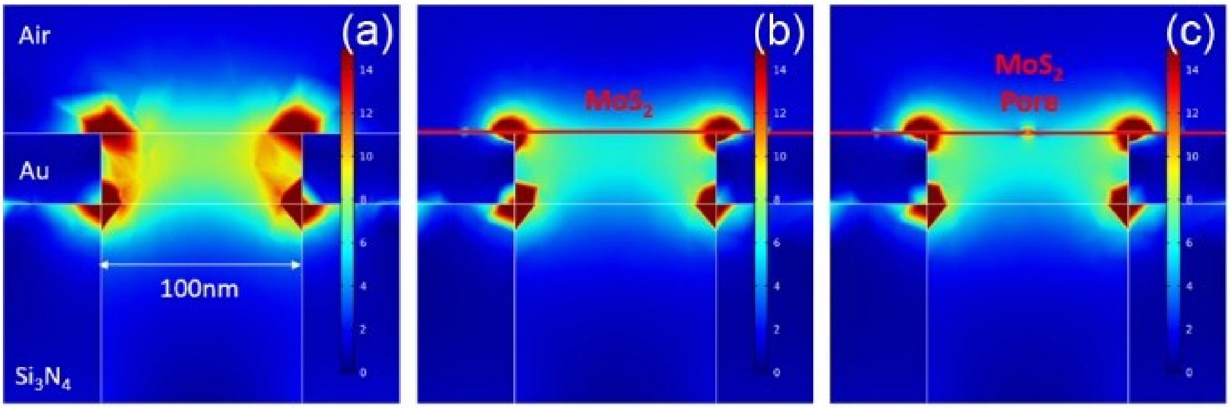

**Figure S4.** *FEM Simulations of MoS2 on top of a metallic nanohole. (a) 100 nm hole on a* $Si_3N_4$ *membrane with 50 nm Au film on top; (b) the metallic hole with* $MoS_2$ *single layer on top; (c) 5 nm hole into* $MoS_2$ *layer.*

Here we also report the simulation on a completely dielectric 3D antenna with the same geometry of the one investigated in the main text. Fig. S5 illustrates how no enhancement can be achieved into the dielectric hole. A slight field confinement is achieved once a hole into the $MoS_2$ layer is created. This is due to the high refractive index of the $MoS_2$ material and the obtained value is one order of magnitude lower respect to the case of plasmonic hole.

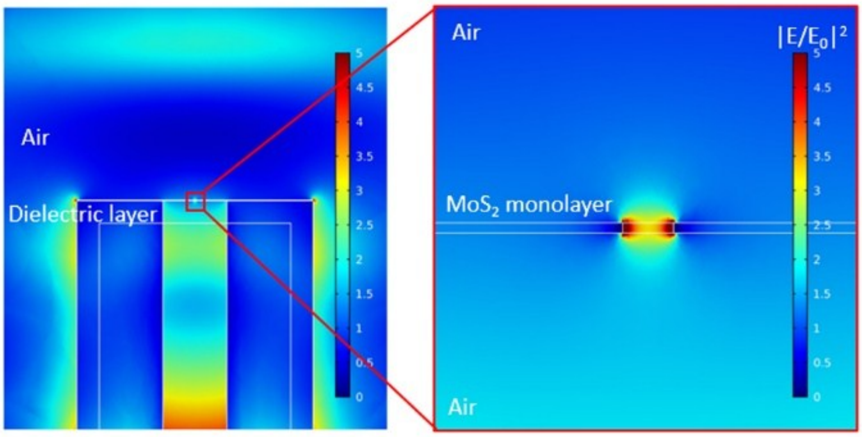

**Figure S5.** *FEM Simulations of* $MoS_2$ *on top of a dielectric 3D antenna.*

## 3. Fabrication of metallic nanoholes

The fabrication of the metallic nanoholes follows simple and robust procedures for the 2D and 3D geometry. In both cases the substrate was a $Si_3N_4$ membrane (50 nm thick) prepared on a Silicon chip. The 2D holes have been prepared by means of FIB milling with a current of 80 pA. After the milling a thin layer of gold, ca. 50 nm, has been deposited on the top side of the membrane. The fabrication of 3D nanoholes array follows the procedure illustrated in Ref. 41 and 42 of the main manuscript and used by our group in several recent papers. A thin layer of S1813 optical resist is spinned on top of the membrane with a final thickness equal to the height of the structure we want to obtain. This layer is exposed by secondary electron during the FIB milling of the nanoholes from the bottom of the membrane, and after the development in acetone and a final metal deposition (ca. 40 nm) a 3D hollow antenna is obtained. All the samples have be treated in $O_2$ plasma before the $MoS_2$ anchoring. As reported in the simulations, for the Raman measurement we used 3D antennas with a final height of 400 nm and a diameter of 150 nm.

## 4. Additional images of $MoS_2$ flakes over 2D and 3D plasmonic nanoholes

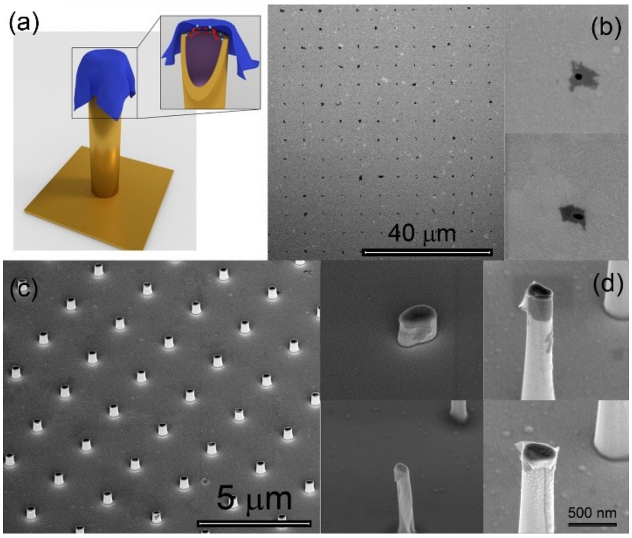

**Figure S7.** *SEM Micrographs of $MoS_2$ flakes deposited over plasmonic nanoholes by means of dithiol anchoring.*

## 5. Analysis of the Raman spectrum – Map from array of deposited $MoS_2$ flakes

In order to assess the number of atomic layers that can be deposited following the proposed method we performed and analysis on the Raman spectrum in terms of $\Delta f$ between the $E^1_{2g}$ and $A_{1g}$ $MoS_2$ modes. Data collected from a 256 antennas integrated with $MoS_2$ flakes have been used. As reported in the main text, 227 antennas result to be decorated with $MoS_2$ with different number of layers. We consider a single layer deposition when $\Delta f$ is below 20 $cm^{-1}$, while 2 layers and more than 3 layers correspond to 21-23 $cm^{-1}$ and more than 23 $cm^{-1}$ respectively. All the spectrum have been analysed by fitting the two Raman modes peaks with a Lorentzian function. All spectrums have been collected with an excitation wavelength of 532 nm. Representative examples of the performed analysis are reported in Fig. S8. As can be seen, it possible to clearly discriminate among the 3 cases.

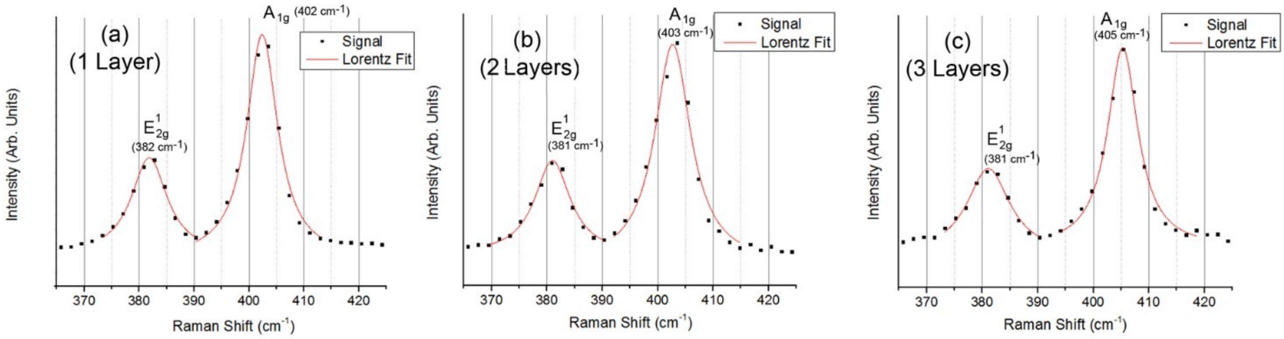

**Figure S8.** *Examples of data analysis on Raman spectrum. (a) Typical spectrum from a single layer $MoS_2$ flake; (b) Spectrum from a 2 layers flake; (c) Spectrum from 3 or more layers.*

Here we also report the obtained spectrum in the case of AuNPs over the flakes for the excitation laser of 532 nm and the spectrum reported in the main text where the data are illustrated in the same scale bar.

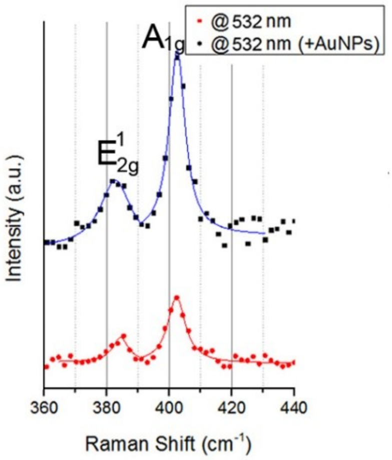

***Figure S9***. *Raman analysis on $MoS_2$ deposited on 3D metallic antennas (@532nm). Raman spectra of the same nanoantenna decorated with a $MoS_2$ flake before and after AuNP growth. Solid lines correspond to Lorentz curve fits, and dots correspond to experimental data.*

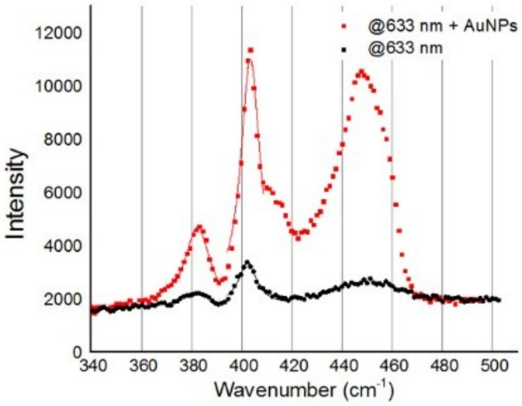

***Figure S10***. *Raman analysis on $MoS_2$ deposited on 3D metallic antennas (@633nm). Raman spectra of the same nanoantenna decorated with a $MoS_2$ flake before and after AuNP growth. Solid lines correspond to Lorentz curve fits, and dots correspond to experimental data.*

## 6. Examples of AuNPs growth on $MoS_2$ flakes

As reported in the main text, the nucleation of AuNPs on $MoS_2$ flakes and nanopores is a controllable procedure with some critical aspects mainly related to the quality of the flakes (i.e. number of layers) and to the incubation-time during nanoparticles growth. In the following micrographs, we reported some examples of AuNPs nucleation with longer time of incubation, up to minutes, where it’s possible to observe the increasing number and dimension of the particles. In the last two SEM micrographs is also possible to observe that the nanoparticles grow on multilayer flakes following preferentially the edges of the material.

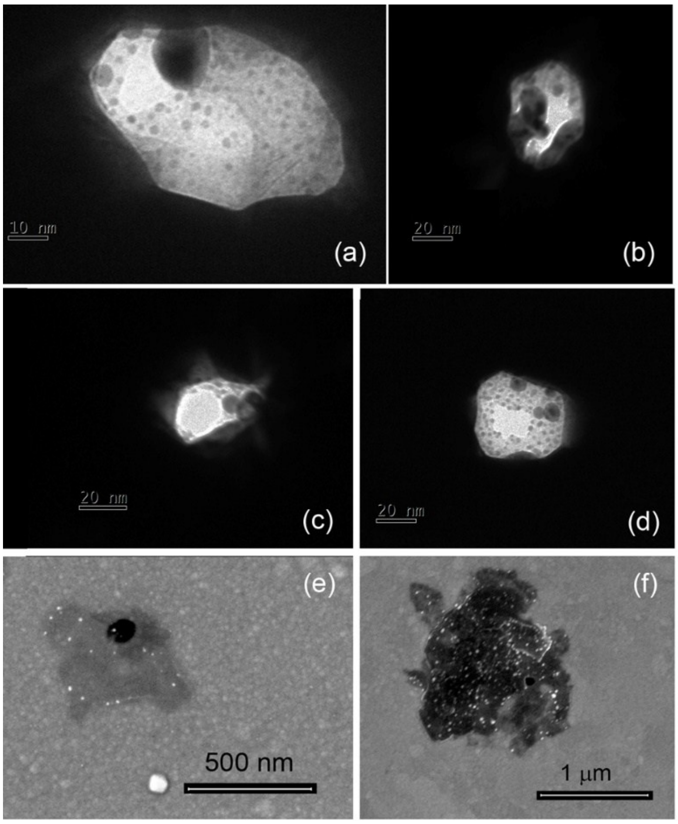

**Figure S11.** *Examples of TEM and SEM micrographs of AuNPs growth on $MoS_2$ flakes (with nanoholes); (a- d) TEM illustrating the AuNPs nucleation for increasing incubation time up to 1 minutes; (e – f) SEM micrographs illustrating bigger AuNPs when incubated for 2 and 3 minutes respectively. .*